Evaluation of a Multiple Model Adaptive Estimation Scheme for Space Vehicle's Enhanced Navigation Solution

Quang M. Lam[1]
Orbital Sciences Corporation
Dulles, VA 20166

John L. Crassidis[2]
University at Buffalo, State University of New York
Amherst, NY 14260-4400

This paper is mainly motivated by the outcome of a previous study carried out by the same authors on the subject of attitude estimation via a multiple model adaptive estimation (MMAE) scheme and serves as the follow-up study to further evaluate the potential of the MMAE scheme subject to higher fidelity models of both sensors and operating environments. The investigation carried out in this paper is aimed at answering the following design questions: (1) Will navigation solution mixing via MMAE truly offer an enhanced solution? (2) Will the MMAE architecture be more suitable for the multi-sensors (i.e., two star trackers, three-axis gyros, image-based sensors, etc) data mixing versus a single Extended Kalman Filter (EKF) design? (3) Will noise extraction and identification via MMAE offer a path to employ low-cost low-grade Micro-Electro-Mechanical Systems (MEMS) sensors? (4) Is it worth our while to consider the MMAE scheme as possible solution for future space vehicle subject to performance enhancement with lower grade and lower cost navigation sensors? The multiple sensors mixing via real-time adaptive mixing coefficients and autonomous switching among these on-board sensors at various operating conditions of a space vehicle's typical mission profile are also used as part of the design objectives in order to realistically evaluate the MMAE solution.

1.0 INTRODUCTION

The attitude determination systems (ADS) of the majority of earth observation missions traditionally employ a six state ADS Kalman filter (e.g., see Lefferts et al [1]) which calibrates the gyro bias error and star tracker attitude error by fusing both star tracker and gyro data in a "bootstrap" fashion to determine the spacecraft attitude. An ADS filter with a higher dimension state vector is simply not needed for these types of missions because of its low orbit rate, less stringent attitude knowledge requirements and high quality ADS sensors (i.e., gyros and star trackers selected for these missions are high grade components). As a result, onboard ADS Kalman filters, with a larger dimension state vector applied to the spacecraft attitude determination system, have been rarely observed. Large state dimensioned ADS filters are normally applied to ground-based software systems for telemetry data processing to fully examine the on-orbit sensor performance.

Stringent attitude knowledge requirements together with spacecraft agility performance specifications demanded by present and future missions have altered such a design tradition and presented a greater design challenge to ADS designers. These include (i) how to separate scale factor errors stability from bias drift stability under high rate operating conditions; (ii) how to achieve precision estimation and accurate tracking of these two parameters when they are strongly correlated at high rate condition; (iii) should a multiple filtering architecture be implemented in a scheduling scheme to address mode variations by having each individual filter turned on based on real-time dynamic mode dependency or should a mix of all filters be employed simultaneously; (iv) what are the design options that ADS designers can use to produce adequate ADS systems meeting stringent performance

[1] Senior Scientist, Email: Lam.quang@orbital.com, Senior Member AIAA
[2] Professor, Department of Mechanical & Aerospace Engineering, Email: johnc@eng.buffalo.edu, Associate Fellow AIAA

requirements at milli-arcsec or even micro-arcsec levels while state-of-the art sensing devices such as advanced star trackers only offer a noise equivalent angle (NEA) of 3 arcsec, etc.

This paper is mainly motivated by the outcome of a previous study [2] on the subject of attitude estimation via a multiple model adaptive estimation (MMAE) scheme and serves as the follow-up study to further evaluate the potential of the MMAE scheme subject to higher fidelity models of both sensors and operating environments. The investigation carried out in this paper is aimed at answering the following design questions: (1) Will navigation solution mixing via MMAE truly offer an enhanced solution? (2) Will the MMAE architecture be more suitable for the multi-sensors (i.e., two star trackers, three-axis gyros, image-based sensors, etc) data mixing vs a single Extended Kalman Filter (EKF) design? (3) Is it worth our while to consider the MMAE scheme as possible solution for future space vehicle subject to performance enhancement with lower grade and lower cost navigation sensors? The multiple sensors mixing via real-time adaptive mixing coefficients and autonomous switching among these on-board sensors at various operating conditions of a space vehicle's typical mission profile are also used as part of the design objectives in order to realistically evaluate the MMAE solution.

2.0 Problem Statement and Research Motivation

The attitude solution mixing via an MMAE scheme (e.g., [2]) or quaternion averaging (e.g., see [3]) tends to offer an enhanced attitude solution. This paper closely examines the attitude (or navigation) solution mixing via the MMAE scheme developed in [2]. The mixing of multiple state estimate vectors produced by the multiple EKFs via a modified mixing coefficient is one of the key design technique investigated by this paper. The real-time dynamic mixing coefficients are implemented using the processing scheme developed by the Interacting Multiple Model (IMM) (e.g., see [4] and [5]) rather than the MMAE scheme. The reason for this mixing design is due to the dynamic probability assignment needed for the EKF models to be allocated in real-time.

The smooth transition among various operating "modes" and sensor data mixing of external aiding sources (i.e., two star trackers and image based sensors) as measurement update to the filter dynamics being propagated via compensated gyros rate are also closely examined and evaluated. Fidelity models of the star trackers and gyros as well as sensor redundancy (i.e., two star trackers for good coverage mixed with image based sensors and/or altimeter) for data mixing will be implemented to reflect the reality of the mission for a better evaluation of the MMAE concept.

3.0 Development of a 15 State Extended Kalman Filter

3.1 Quaternion Parameterization and Gyro Model

For spacecraft attitude estimation, the quaternion has been the most widely used attitude parameterization [1]. The quaternion is given by a four-dimensional vector, defined as

$$\mathbf{q} = \begin{bmatrix} \mathbf{q}_{13} \\ q_4 \end{bmatrix} \tag{1}$$

with $\mathbf{q}_{13} \equiv \begin{bmatrix} q_1 & q_2 & q_3 \end{bmatrix}^T = \mathbf{d}\sin(\vartheta/2)$ and $q_4 = \cos(\vartheta/2)$, where $\mathbf{d}$ is the unit Euler axis and ϑ is the rotation angle. Because a four-dimensional vector is used to describe three dimensions, the quaternion components cannot be independent of each other. The quaternion satisfies a single constraint given by $\mathbf{q}^T\mathbf{q} = 1$. The attitude matrix is related to the quaternion by

$$A(\mathbf{q}) = \Xi^T(\mathbf{q})\Psi(\mathbf{q}) \tag{2}$$

with

$$\Xi(\mathbf{q}) \equiv \begin{bmatrix} q_4 I_{3\times 3} + [\mathbf{q}_{13}\times] \\ -\mathbf{q}_{13}^T \end{bmatrix} \tag{3a}$$

$$\Psi(\mathbf{q}) \equiv \begin{bmatrix} q_4 I_{3\times 3} - [\mathbf{q}_{13}\times] \\ -\mathbf{q}_{13}^T \end{bmatrix} \tag{3b}$$

where $I_{3\times 3}$ is a 3×3 identity matrix and $[\mathbf{q}_{13}\times]$ is the cross product matrix, defined by

$$[\mathbf{q}_{13}\times] \equiv \begin{bmatrix} 0 & -q_3 & q_2 \\ q_3 & 0 & -q_1 \\ -q_2 & q_1 & 0 \end{bmatrix} \tag{4}$$

For small angles the vector part of the quaternion is approximately equal to half angles [6].

The quaternion kinematics equation is given by

$$\dot{\mathbf{q}} = \frac{1}{2}\Xi(\mathbf{q})\boldsymbol{\omega} \tag{5}$$

where $\boldsymbol{\omega}$ is the three-component angular rate vector. A major advantage of using the quaternion is that the kinematics equation is linear in the quaternion and is also free of singularities. Another advantage of the quaternion is that successive rotations can be accomplished using quaternion multiplication. Here the convention of [6] is adopted, where the quaternions are multiplied in the same order as the attitude matrix multiplication, in contrast to the usual convention established by Hamilton. A successive rotation is written using $A(\mathbf{q}')A(\mathbf{q}) = A(\mathbf{q}'\otimes\mathbf{q})$. The composition of the quaternions is bilinear, with

$$\mathbf{q}'\otimes\mathbf{q} = [\Psi(\mathbf{q}') \quad \mathbf{q}']\mathbf{q} = [\Xi(\mathbf{q}) \quad \mathbf{q}]\mathbf{q}' \tag{6}$$

Also, the inverse quaternion is given by $\mathbf{q}^{-1} \equiv \begin{bmatrix} -\mathbf{q}_{13}^T & q_4 \end{bmatrix}^T$, with $A(\mathbf{q}^{-1}) = A^T(\mathbf{q})$. Note that $\mathbf{q}\otimes\mathbf{q}^{-1} = [0 \quad 0 \quad 0 \quad 1]^T$, which is the identity quaternion.

A common sensor that measures the angular rate is a rate integrating gyro. For this sensor, a widely used three-axis continuous-time model is given by

$$\begin{aligned} \tilde{\boldsymbol{\omega}} &= (I_{3\times 3} + S)\boldsymbol{\omega} + \mathbf{b} + \boldsymbol{\eta}_v \\ \dot{\mathbf{b}} &= \boldsymbol{\eta}_u \\ \dot{\mathbf{s}} &= \boldsymbol{\eta}_s \\ \dot{\mathbf{k}}_U &= \boldsymbol{\eta}_U \\ \dot{\mathbf{k}}_L &= \boldsymbol{\eta}_L \\ S &\equiv \begin{bmatrix} s_1 & k_{U1} & k_{U2} \\ k_{L1} & s_2 & k_{U3} \\ k_{L2} & k_{L3} & s_3 \end{bmatrix} \end{aligned} \tag{7}$$

where $\tilde{\boldsymbol{\omega}}$ is the measured rate, $\mathbf{b}$ is the drift, S is a matrix of scale factors $\mathbf{s}$ and misalignments $\mathbf{k}_U$ and $\mathbf{k}_L$, and $\boldsymbol{\eta}_v$ (i.e., angular random walk, ARW), $\boldsymbol{\eta}_u$ (i.e., rate random walk, RRW) and $\boldsymbol{\eta}_s$, $\boldsymbol{\eta}_U$ and $\boldsymbol{\eta}_L$ are independent zero-mean Gaussian white-noise processes with

$$
\begin{aligned}
E\left\{\boldsymbol{\eta}_v(t)\boldsymbol{\eta}_v^T(\tau)\right\} &= \sigma_v^2\delta(t-\tau)I_{3\times3}\\
E\left\{\boldsymbol{\eta}_u(t)\boldsymbol{\eta}_u^T(\tau)\right\} &= \sigma_u^2\delta(t-\tau)I_{3\times3}\\
E\left\{\boldsymbol{\eta}_s(t)\boldsymbol{\eta}_s^T(\tau)\right\} &= \sigma_s^2\delta(t-\tau)I_{3\times3}\\
E\left\{\boldsymbol{\eta}_U(t)\boldsymbol{\eta}_U^T(\tau)\right\} &= \sigma_U^2\delta(t-\tau)I_{3\times3}\\
E\left\{\boldsymbol{\eta}_L(t)\boldsymbol{\eta}_L^T(\tau)\right\} &= \sigma_L^2\delta(t-\tau)I_{3\times3}
\end{aligned}
\tag{8}
$$

where E{ } denotes expectation and $\delta(t-\tau)$ is the Dirac-delta function.

3.2 Kalman Filtering for Attitude Estimation

This section provides a review of the equations involved for spacecraft attitude estimation using the Kalman filter. The measurements are assumed to be given for a star tracker determined Kalman filter. To within first-order the quaternion measurements can be modeled by

$$
\tilde{\mathbf{q}} = \mathbf{q} + \frac{1}{2}\Xi(\mathbf{q})\,\mathbf{v} \tag{9}
$$

where $\tilde{\mathbf{q}}$ is the measurement quaternion and $\mathbf{v}$ is a zero-mean Gaussian process with covariance R. Note that $\mathbf{v}$ is not a stationary process and R is determined from the attitude error-covariance of the attitude determination process [4]. Also, to within first-order the quaternion normalization constraint is maintained with this measurement model. A summary of the extended Kalman filter (EKF) for attitude estimation, including gyro drifts and scale factors, is shown in Table 1. All symbols and characters with a hat over them signify estimates. The variables P_k^+ and P_k^- denote the updated and propagated error-covariance at time t_k, respectively; K_k is the Kalman gain; the first three components of $\Delta\hat{\mathbf{x}}$, denoted by $\boldsymbol{\delta\hat{\alpha}}$, are the small-attitude error estimates, and the vector $\hat{\mathbf{s}}$ denotes the diagonal elements of the estimate scale factor matrix, $\hat{S}$. Note that the propagated values for the gyro drift and scale factors are given by their previous time values.

We now derive the $F(t)$ and $G(t)$ matrices. Here it is assumed that $(I_{3\times3}+S)^{-1} \approx (I_{3\times3}-S)$, which is valid for small S. A multiplicative error quaternion is used to derive the attitude errors:

$$
\boldsymbol{\delta q} = \mathbf{q}\otimes\hat{\mathbf{q}}^{-1} \approx \begin{bmatrix} 0.5\boldsymbol{\delta\alpha} \\ 1 \end{bmatrix} \tag{10}
$$

where $\boldsymbol{\delta\alpha}$ is the vector of small attitude (roll, pitch and yaw) attitude errors. The error-kinematics follow [1]

$$
\boldsymbol{\delta\dot{\alpha}} = -\left[\hat{\boldsymbol{\omega}}\times\right]\boldsymbol{\delta\alpha} + \boldsymbol{\delta\omega} \tag{11}
$$

where $\boldsymbol{\delta\omega} \equiv \boldsymbol{\omega} - \hat{\boldsymbol{\omega}}$. From Eq. (7) we have

$$
\begin{aligned}
\boldsymbol{\omega} &= (I_{3\times3}-S)\tilde{\boldsymbol{\omega}} - (I_{3\times3}-S)\mathbf{b} - (I_{3\times3}-S)\boldsymbol{\eta}_v\\
\hat{\boldsymbol{\omega}} &= \left(I_{3\times3}-\hat{S}\right)\tilde{\boldsymbol{\omega}} - \left(I_{3\times3}-\hat{S}\right)\hat{\mathbf{b}}
\end{aligned}
\tag{12}
$$

Then $\boldsymbol{\delta\omega}$ is given by

$$\begin{aligned}\boldsymbol{\delta\omega} &= -\Delta S\,\tilde{\boldsymbol{\omega}} - \Delta\mathbf{b} + \left(\Delta S + \hat{S}\right)\left(\Delta\mathbf{b} + \hat{\mathbf{b}}\right) - \hat{S}\,\hat{\mathbf{b}} \\ &\quad -\left(I_{3\times 3} - \hat{S} - \Delta S\right)\boldsymbol{\eta}_v\end{aligned} \tag{13}$$

where $\Delta S \equiv S - \hat{S}$ and $\Delta\mathbf{b} \equiv \mathbf{b} - \hat{\mathbf{b}}$. Ignoring second-order terms leads to

$$\begin{aligned}\boldsymbol{\delta\omega} &= \left(I_{3\times 3} - \hat{S}\right)\Delta\mathbf{b} - \mathrm{diag}\left(\tilde{\boldsymbol{\omega}} - \hat{\mathbf{b}}\right)\Delta\mathbf{s} \\ &\quad -\hat{U}\,\Delta\mathbf{k}_U - \hat{L}\,\Delta\mathbf{k}_L - \left(I_{3\times 3} - \hat{S}\right)\boldsymbol{\eta}_v \\ \hat{U} &= \begin{bmatrix} \tilde{\omega}_2 - \hat{b}_2 & \tilde{\omega}_3 - \hat{b}_3 & 0 \\ 0 & 0 & \tilde{\omega}_3 - \hat{b}_3 \\ 0 & 0 & 0 \end{bmatrix} \\ \hat{L} &= \begin{bmatrix} 0 & 0 & 0 \\ \tilde{\omega}_1 - \hat{b}_1 & 0 & 0 \\ 0 & \tilde{\omega}_1 - \hat{b}_1 & \tilde{\omega}_2 - \hat{b}_2 \end{bmatrix}\end{aligned} \tag{14}$$

where diag denotes a diagonal matrix, $\Delta\mathbf{s}$ is a vector of the diagonal elements of ΔS, and $\Delta\mathbf{k}_U$ and $\Delta\mathbf{k}_L$ correspond to the upper and lower off-diagonal elements of ΔS. Hence, the matrices $F(t)$, $G(t)$ and $Q(t)$ are given by

$$\begin{aligned}F &= \begin{bmatrix} -\left[\hat{\boldsymbol{\omega}}\times\right] & -\left(I_{3\times 3} - \hat{S}\right) & \mathrm{diag}\left(\tilde{\boldsymbol{\omega}} - \hat{\mathbf{b}}\right) & \hat{U} & \hat{L} \\ 0_{3\times 3} & 0_{3\times 3} & 0_{3\times 3} & 0_{3\times 3} & 0_{3\times 3} \\ 0_{3\times 3} & 0_{3\times 3} & 0_{3\times 3} & 0_{3\times 3} & 0_{3\times 3} \\ 0_{3\times 3} & 0_{3\times 3} & 0_{3\times 3} & 0_{3\times 3} & 0_{3\times 3} \\ 0_{3\times 3} & 0_{3\times 3} & 0_{3\times 3} & 0_{3\times 3} & 0_{3\times 3} \end{bmatrix} \\ G &= \begin{bmatrix} -\left(I_{3\times 3} - \hat{S}\right) & 0_{3\times 3} & 0_{3\times 3} & 0_{3\times 3} & 0_{3\times 3} \\ 0_{3\times 3} & I_{3\times 3} & 0_{3\times 3} & 0_{3\times 3} & 0_{3\times 3} \\ 0_{3\times 3} & 0_{3\times 3} & I_{3\times 3} & 0_{3\times 3} & 0_{3\times 3} \\ 0_{3\times 3} & 0_{3\times 3} & 0_{3\times 3} & I_{3\times 3} & 0_{3\times 3} \\ 0_{3\times 3} & 0_{3\times 3} & 0_{3\times 3} & 0_{3\times 3} & I_{3\times 3} \end{bmatrix} \\ Q &= \begin{bmatrix} \sigma_v^2 I_{3\times 3} & 0_{3\times 3} & 0_{3\times 3} & 0_{3\times 3} & 0_{3\times 3} \\ 0_{3\times 3} & \sigma_u^2 I_{3\times 3} & 0_{3\times 3} & 0_{3\times 3} & 0_{3\times 3} \\ 0_{3\times 3} & 0_{3\times 3} & \sigma_s^2 I_{3\times 3} & 0_{3\times 3} & 0_{3\times 3} \\ 0_{3\times 3} & 0_{3\times 3} & 0_{3\times 3} & \sigma_U^2 I_{3\times 3} & 0_{3\times 3} \\ 0_{3\times 3} & 0_{3\times 3} & 0_{3\times 3} & 0_{3\times 3} & \sigma_L^2 I_{3\times 3} \end{bmatrix}\end{aligned} \tag{15}$$

Table 1. EKF For Attitude Estimation

Initialize	$\hat{\mathbf{q}}(t_0)=\hat{\mathbf{q}}_0, \quad \hat{\mathbf{b}}(t_0)=\hat{\mathbf{b}}_0, \quad \hat{\mathbf{s}}(t_0)=\hat{\mathbf{s}}_0$ $\hat{\mathbf{k}}_U(t_0)=\hat{\mathbf{k}}_{U0}, \quad \hat{\mathbf{k}}_L(t_0)=\hat{\mathbf{k}}_{L0}$ $P(t_0)=P_0$
Compute Gain	$K_k=P_k^- H^T\left(H\,P_k^- H^T+R_k\right)^{-1}$ $H=\begin{bmatrix} I_{3\times3} & 0_{3\times3} & 0_{3\times3} & 0_{3\times3} & 0_{3\times3}\end{bmatrix}$
Update	$P_k^+=\left(I_{15\times15}-K_kH\right)P_k^-$ $\Delta\hat{\mathbf{x}}_k^+=2K_k\,\Xi^T\left(\hat{\mathbf{q}}_k^-\right)\tilde{\mathbf{q}}_k$ $\Delta\hat{\mathbf{x}}_k^+\equiv\begin{bmatrix}\boldsymbol{\delta\hat{\alpha}}_k^{+T} & \Delta\hat{\mathbf{b}}_k^{+T} & \Delta\hat{\mathbf{s}}_k^{+T} & \Delta\hat{\mathbf{k}}_{Uk}^{+T} & \Delta\hat{\mathbf{k}}_{Lk}^{+T}\end{bmatrix}^{TT}$ $\hat{\mathbf{q}}_k^+=\hat{\mathbf{q}}_k^-+\frac{1}{2}\Xi\left(\hat{\mathbf{q}}_k^-\right)\boldsymbol{\delta\hat{\alpha}}_k^{+T}$, re-normalize $\hat{\mathbf{b}}_k^+=\hat{\mathbf{b}}_k^-+\Delta\hat{\mathbf{b}}_k^+$ $\hat{\mathbf{s}}_k^+=\hat{\mathbf{s}}_k^-+\Delta\hat{\mathbf{s}}_k^+$ $\hat{\mathbf{k}}_{Uk}^+=\hat{\mathbf{k}}_{Uk}^-+\Delta\hat{\mathbf{k}}_{Uk}^+$ $\hat{\mathbf{k}}_{Lk}^+=\hat{\mathbf{k}}_{Lk}^-+\Delta\hat{\mathbf{k}}_{Lk}^+$
Propagate	$\hat{\boldsymbol{\omega}}(t)=\left[I_{3\times3}-\hat{S}(t)\right]\left[\tilde{\boldsymbol{\omega}}(t)-\hat{\mathbf{b}}(t)\right]$ $\dot{\hat{\mathbf{q}}}=\frac{1}{2}\Xi\left[\hat{\mathbf{q}}(t)\right]\hat{\boldsymbol{\omega}}(t)$ $\dot{\hat{\mathbf{b}}}(t)=\mathbf{0}$ $\dot{\hat{\mathbf{s}}}(t)=\mathbf{0}$ $\dot{\hat{\mathbf{k}}}_U=\mathbf{0}$ $\dot{\hat{\mathbf{k}}}_L=\mathbf{0}$ $\dot{P}(t)=F(t)P(t)+P(t)F^T(t)+G(t)Q(t)G^T(t)$

A discrete-time propagation of the quaternion and error-covariance is possible (see [5] for details). The discrete-time covariance propagation is given by

$$P_k^- = \Phi_k P_k^+ \Phi_k^T + Q_k \tag{16}$$

where Φ_k and Q_k are discrete-time state transition and process-noise covariance matrices, respectively. For small sampling intervals the discrete process noise matrix is well approximated by (also see [8])

$$\Phi_k \approx I_{15\times15} + \Delta t\, F(t) + \frac{1}{2}\Delta t^2\, F^2(t)$$

$$Q_k \approx \begin{bmatrix} \left(\sigma_v^2 + \frac{1}{3}\sigma_u^2\Delta t^2\right)\Delta t\, I_{3\times3} + \frac{1}{3}\sigma_s^2\Delta t^3\Omega^2\left(\hat{\boldsymbol{\omega}}_k\right) & -\frac{1}{2}\sigma_u^2\Delta t^2 I_{3\times3} & -\frac{1}{2}\sigma_s^2\Delta t^2\Omega^2\left(\hat{\boldsymbol{\omega}}_k\right) & \frac{1}{2}\sigma_U^2\Delta t^2\hat{U} & \frac{1}{2}\sigma_L^2\Delta t^2\hat{L} \\ -\frac{1}{2}\sigma_u^2\Delta t^2 I_{3\times3} & \sigma_u^2\Delta t^2 I_{3\times3} & 0_{3\times3} & 0_{3\times3} & 0_{3\times3} \\ -\frac{1}{2}\sigma_s^2\Delta t^2\Omega^2\left(\hat{\boldsymbol{\omega}}_k\right) & 0_{3\times3} & \sigma_v^2\Delta t^2 I_{3\times3} & 0_{3\times3} & 0_{3\times3} \\ \frac{1}{2}\sigma_U^2\Delta t^2\hat{U}^T & 0_{3\times3} & 0_{3\times3} & \sigma_U^2\Delta t^2 I_{3\times3} & 0_{3\times3} \\ \frac{1}{2}\sigma_L^2\Delta t^2\hat{L}^T & 0_{3\times3} & 0_{3\times3} & 0_{3\times3} & \sigma_L^2\Delta t^2 I_{3\times3} \end{bmatrix} \tag{17}$$

where Δt is the sampling interval and $\Omega\left(\hat{\boldsymbol{\omega}}_k\right)$ is a diagonal matrix made up of the elements of the estimate rate.

4.0 Multiple-Model Adaptive Estimation

4.1 MMAE Formulation

Multiple-model adaptive estimation described in [2] is a recursive estimator that uses a bank of filters that depend on some unknown parameters. In our case these parameters are the process noise covariance, denoted by the vector $\mathbf{p}$, which is assumed to be constant (at least throughout the interval of adaptation). Note that we do not necessarily need to make the stationary assumption for the state and/or output processes though, i.e. time varying state and output matrices can be used. A set of distributed elements is generated from some known probability density function (pdf) of $\mathbf{p}$, denoted by $p(\mathbf{p})$, to give $\left\{\mathbf{p}^{(\ell)}; \ell = 1,\ldots,M\right\}$. The goal of the estimation process is to determine the conditional pdf of the ℓ^{th} element of $\mathbf{p}^{(\ell)}$ given the current-time measurement $\tilde{\mathbf{y}}_k$. Application of Bayes rule yields

$$p\left(\mathbf{p}^{(\ell)} \mid \tilde{\mathbf{Y}}_k\right) = \frac{p\left(\tilde{\mathbf{Y}}_k \mid \mathbf{p}^{(\ell)}\right) p\left(\mathbf{p}^{(\ell)}\right)}{\sum_{j=1}^{M} p\left(\tilde{\mathbf{Y}}_k \mid \mathbf{p}^{(j)}\right) p\left(\mathbf{p}^{(j)}\right)} \tag{18}$$

where $\tilde{\mathbf{Y}}_k$ denotes the sequence $\left\{\tilde{\mathbf{y}}_0, \tilde{\mathbf{y}}_1, \ldots, \tilde{\mathbf{y}}_k\right\}$. The *a posteriori* probabilities can be computed through

$$\begin{aligned} p\left(\mathbf{p}^{(\ell)} \mid \tilde{\mathbf{Y}}_k\right) &= \frac{p\left(\tilde{\mathbf{y}}_k, \mathbf{p}^{(\ell)} \mid \tilde{\mathbf{Y}}_{k-1}\right)}{p\left(\tilde{\mathbf{y}}_k \mid \tilde{\mathbf{Y}}_{k-1}\right)} \\ &= \frac{p\left(\tilde{\mathbf{y}}_k \mid \hat{\mathbf{x}}_k^{-(\ell)}\right) p\left(\mathbf{p}^{(\ell)} \mid \tilde{\mathbf{Y}}_{k-1}\right)}{\sum_{j=1}^{M} p\left(\tilde{\mathbf{y}}_k \mid \hat{\mathbf{x}}_k^{-(j)}\right) p\left(\mathbf{p}^{(j)} \mid \tilde{\mathbf{Y}}_{k-1}\right)} \end{aligned} \tag{19}$$

where $\hat{\mathbf{x}}_k^{-(\ell)}$ denotes the propagated state estimate of the ℓ^{th} Kalman filter. Note that the denominator of Eq. (19) is just a normalizing factor to ensure that $p\left(\mathbf{p}^{(\ell)} \mid \tilde{\mathbf{Y}}_k\right)$ is a pdf. The recursion formula can now be cast into a set of defined weights $\varpi_k^{(\ell)}$

$$\varpi_k^{(\ell)} = \varpi_{k-1}^{(\ell)}\, p\left(\tilde{\mathbf{y}}_k \mid \hat{\mathbf{x}}_k^{-(\ell)}\right)$$
$$\varpi_k^{(\ell)} \leftarrow \frac{\varpi_k^{(\ell)}}{\sum_{j=1}^{M} \varpi_k^{(\ell)}} \tag{20}$$

where $\varpi_k^{(\ell)} \equiv p\left(\mathbf{p}^{(\ell)} \mid \tilde{\mathbf{Y}}_{k-1}\right)$. The weights are initialized to $\varpi_0^{(\ell)} = 1/M$ for $\ell = 1, 2, \ldots, M$. Note that $p\left(\tilde{\mathbf{y}}_k \mid \hat{\mathbf{x}}_k^{-(\ell)}\right)$ denotes the likelihood function.

The conditional mean estimate is the weighted sum of the parallel filter estimates

$$\hat{\mathbf{x}}_k^- = \sum_{j=1}^{M} \varpi_k^{(j)} \hat{\mathbf{x}}_k^{-(j)} \tag{21}$$

Also, the error covariance of the state estimate can be computed using

$$P_k^- = \sum_{j=1}^{M} \varpi_k^{(j)} \left(\hat{\mathbf{x}}_k^{-(j)} - \hat{\mathbf{x}}_k^-\right)\left(\hat{\mathbf{x}}_k^{-(j)} - \hat{\mathbf{x}}_k^-\right)^T \tag{22}$$

The specific estimate for $\mathbf{p}$ at time t_k, denoted by $\hat{\mathbf{p}}_k$, and error covariance, denoted by Z_k, are given by

$$\hat{\mathbf{p}}_k = \sum_{j=1}^{M} \varpi_k^{(j)} \mathbf{p}^{(j)} \tag{23a}$$

$$Z_k = \sum_{j=1}^{M} \varpi_k^{(j)} \left(\mathbf{p}^{(j)} - \hat{\mathbf{p}}_k\right)\left(\mathbf{p}^{(j)} - \hat{\mathbf{p}}_k\right)^T \tag{23b}$$

Equation (23b) can be used to define 3σ bounds on the estimate $\hat{\mathbf{p}}_k$.

4.2 Attitude Likelihood Function

This section derives the likelihood function for the MMAE algorithm using quaternion measurements. From Table 1, the measurement residual is defined to be (ignoring the propagated notation for $\hat{\mathbf{q}}$)

$$\mathbf{e} \equiv 2\,\Xi^T\left(\hat{\mathbf{q}}\right)\tilde{\mathbf{q}} \tag{24}$$

which is derived from the vector part of $\tilde{\mathbf{q}} \otimes \hat{\mathbf{q}}^{-1}$ (the factor of 2 is used so that $\mathbf{e}$ represents half-angle residuals). Using Eq. (9) and $\hat{\mathbf{q}} = \mathbf{q} + \frac{1}{2}\Xi^T(\mathbf{q})\delta\boldsymbol{\alpha}$ in Eq. (24) gives

$$\mathbf{e} = 2\left[\Xi^T(\mathbf{q}) + \frac{1}{2}\Xi^T\left(\Xi(\mathbf{q})\delta\boldsymbol{\alpha}\right)\right]\left[\mathbf{q} + \frac{1}{2}\Xi^T(\mathbf{q})\mathbf{v}\right] \tag{25}$$

Using the identity $\Xi^T\left(\Xi(\mathbf{q})\delta\boldsymbol{\alpha}\right) = -[\delta\boldsymbol{\alpha}\times]\Xi^T(\mathbf{q}) - \delta\boldsymbol{\alpha}\,\mathbf{q}^T$ in Eq. (25) leads to

$$\mathbf{e} = \mathbf{v} - \frac{1}{2}[\delta\boldsymbol{\alpha}\times]\mathbf{v} - \delta\boldsymbol{\alpha} \tag{26}$$

where $\Xi^T(\mathbf{q})\Xi(\mathbf{q}) = I_{3\times 3}$, $\Xi^T(\mathbf{q})\mathbf{q} = \mathbf{0}$ and $\mathbf{q}^T\mathbf{q} = 1$ have been used. Therefore, since $\delta\boldsymbol{\alpha}$ and $\mathbf{v}$ are uncorrelated, the covariance of the residual at time t_k, using the propagated values, is given by

$$E\left\{\mathbf{e}_k^-\mathbf{e}_k^{-T}\right\} = H\,P_k^-H^T + R_k \tag{27}$$

where H is defined in Table 1. Therefore the likelihood function is given by

$$\Lambda_\ell \equiv p\left(\tilde{\mathbf{y}}_k \mid \hat{\mathbf{x}}_k^{-(\ell)}\right) = \frac{1}{\left\{\det\left[2\pi\left(H\,P_k^{-(\ell)}H^T + R_k\right)\right]\right\}^{1/2}}\exp\left[-\frac{1}{2}\mathbf{e}_k^{-(\ell)}\left(H\,P_k^{-(\ell)}H^T + R_k\right)^{-1}\mathbf{e}_k^{-(\ell)}\right] \tag{28}$$

which is used to update the weights in the MMAE algorithm.

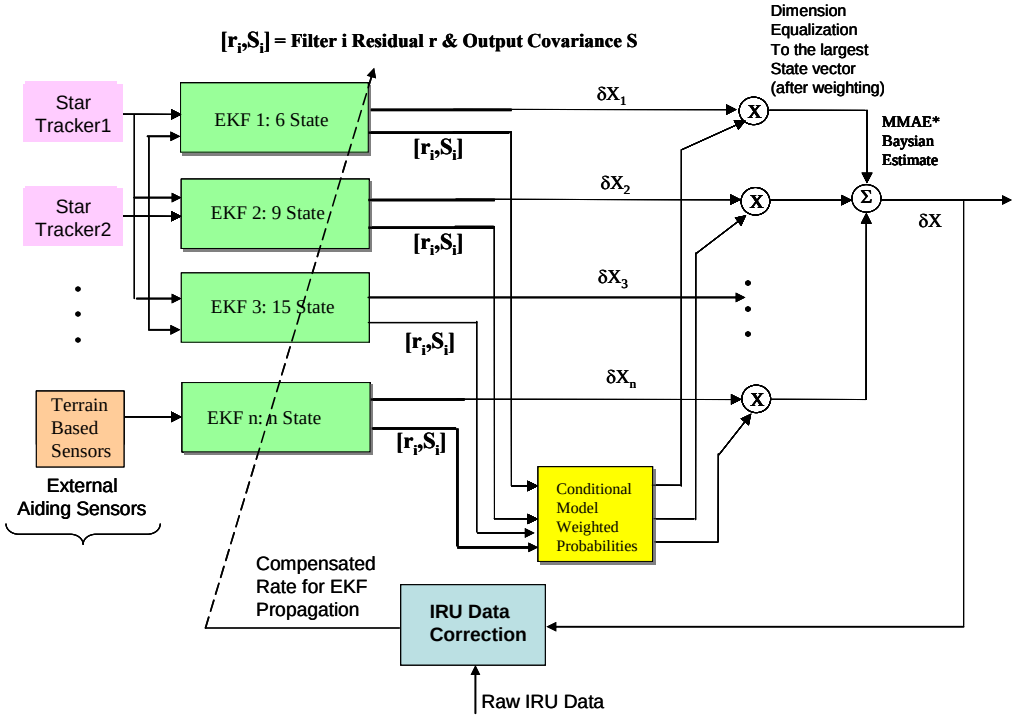

Figure 1. MMAE Architecture Suitable for Multiple Sensors Fusion

4.3 Multiple Model Adaptive Estimation (MMAE) Filtering For Multiple Sensor Fusion Architecture

The linear multiple model filter design framework is now extended into an MMAE scheme wherein the pre-selected α_i coefficients now can be computed on-line using some adaptive computation scheme subject to a performance criterion. The MMAE baseline algorithm described in Section 4.0 is adopted here to enhance the performance of a typical multi-slewing multi-rate operating condition during imaging mode presented early on. The MMAE architecture applied to the multiple model ADS filter is depicted in Figure 1 wherein three ADS filter structures are employed to address the multi-rate/multi-mode situation. The fifteen-state ADS filter is the largest model that is implemented to fully address the attitude error and the gyro high order calibration of bias and fully populated misalignment matrix. The nine-state ADS filter model will address the attitude error and the gyro bias and symmetrical scale factor errors. Finally, the six-state ADS filter model consisting of attitude and gyro bias error is implemented to provide precision attitude determination in the low rate operating condition.

The multi-state mixing of three ADS filters is accomplished using the Interacting Multiple Model (IMM) blending approach ([4] and [5]) expressed as follows:

$$\delta\hat{\mathrm{x}}(\mathrm{n}+1|\mathrm{n}+1)=\sum_{j}\delta\hat{\mathrm{x}}_{\mathrm{j}}(\mathrm{n}+1|\mathrm{n}+1)\mu_{\mathrm{i}|\mathrm{j}}(\mathrm{n}+1) \tag{29}$$

where j=1:m with m being the number of filter models in general. For the scope of this paper, m is set to 3 for 6 state EKF, 9 state EKF, and 15 state EKF, respectively. The mixing coefficient probabilities $\mu_{\mathrm{i|j}}$ are computed as

$$\mu_{\mathrm{i}|\mathrm{j}}(n+1\,|\,n+1)=\mathrm{p}_{\mathrm{ij}}\mu_{\mathrm{i}}(n+1)/\bar{c}_{\mathrm{j}} \tag{30}$$

where

$$\bar{c}_{\mathrm{j}}=\sum_{\mathrm{i}=1}^{\mathrm{r}}\mathrm{p}_{\mathrm{ij}}\mu_{\mathrm{i}}(\mathrm{n}+1) \tag{31}$$

$$\mu_i(n+1)=\frac{1}{c}\Lambda_i(n)\sum_{i=1}^{m}p_{ij}\mu_i(n),\ j=1:m \tag{32}$$

where μ_i computed in equation (32) is also called as the mode probability update, and

$$c=\sum_{j=1}^{m}\Lambda_j(n)\bar{c}_j \tag{33}$$

where Λ_i is the likelihood functions of model I described in equation (28), and p_{ij} is i-j^{th} element of a 3×3 probability transition matrix computed as follows:

$$P_{trans}=\left[\begin{array}{c|c|c} P_{11} & 0.05*(1-P_{11}) & 0.95*(1-P_{11}) \\ \hline 0.05*(1-P_{22}) & P_{22} & 0.95*(1-P_{22}) \\ \hline (1-P_{33})/3 & 2*(1-P_{33})/3 & P_{33} \end{array}\right] \tag{34}$$

P_{ii} will be chosen to reflect mission specific's rate profile. For our study, P_{trans} is selected to be:

$$P_{trans}=\left[\begin{array}{c|c|c} 0.9000 & 0.0050 & 0.0950 \\ \hline 0.0033 & 0.9333 & 0.0633 \\ \hline 0.0677 & 0.1333 & 0.8000 \end{array}\right] \tag{35}$$

5.0 Performance Evaluation & Discussion

In general, at low rate operating condition when the navigation performance impact due to the " participation" of scale factor (SF) errors and misalignment (MA) errors is negligible, designers can select the lower dimension EKF (i.e., 6 state EKF for this study) implemented in a single EKF low rate mode. Similarly, for medium rate and high rate operating conditions, higher dimension EKFs are then selected to account for SF errors and MA errors (i.e., 9 state and 15 state EKFs for this study), and these high dimension EKFs will be implemented in a single EKF mode and individually selected based on the actual rate magnitude signatures (being monitored in real-time.) This implementation can be similarly viewed as the "gain scheduling" approach employed by the control approach counter part. Drawbacks associated with the gain scheduling approach when dealing with nonlinearities, parameter variations, and model orders are still applied to the estimation problem. As a result, an adaptive estimation scheme is still being actively sought.

The main motivation of searching for an enhanced attitude/navigation solution via the multiple model mixing approach is described in Ref. 2. The reason behind employing a combined solution produced by a set of multiple EKFs can be intuitively perceived as "the averaging quaternions" design concept presented in Ref. 3. Here instead of "averaging" all solutions produced by a set of EKFS, we employ the MMAE/IMM scheme to compute a real-time dynamic mixing "probability coefficients" at various range rates allowing the participation of each navigation filter contributing their knowledge at its best based on or dictated by its real-time likelihood function. Therefore, we are not "equally" averaging all solutions to produce a single solution at all time. Rather, we use the best solution produced by the best EKF (dictated by its own dynamic mode probability) in real-time while for the least accurate solutions, they are judiciously being selected (via an MMAE/IMM mixing scheme) for whatever their worth contribution (instead of completely throwing them out under the single EKF implementation!) The following sections will illustrate the effectiveness of the proposed MMAE solution versus a solution produced by a single EKF.

5.1 Performance of a Single Filter (Baseline 15 State EKF)

Figures 1 through 6 show the performance using only the 15 state filter. From Figure 5 it is seen that the 3-sigma bound do not bound one of the estimate errors for the misalignment portion. This is most likely due to low observability in this parameter.

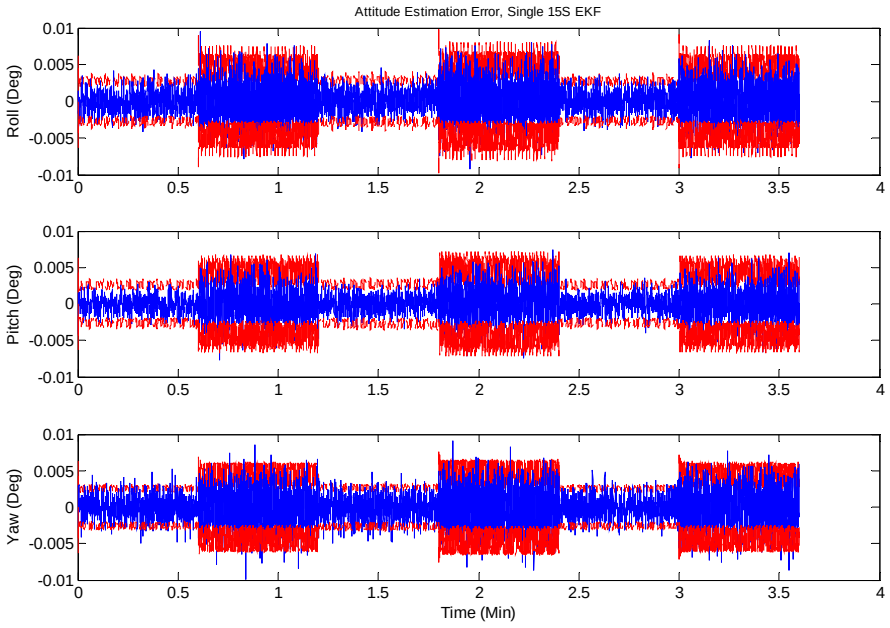

Figure 2. Attitude Estimation Performance of a 15 State Single EKF (1 sigma error: [5.8931 4.7698 6.2053] arcsecs)

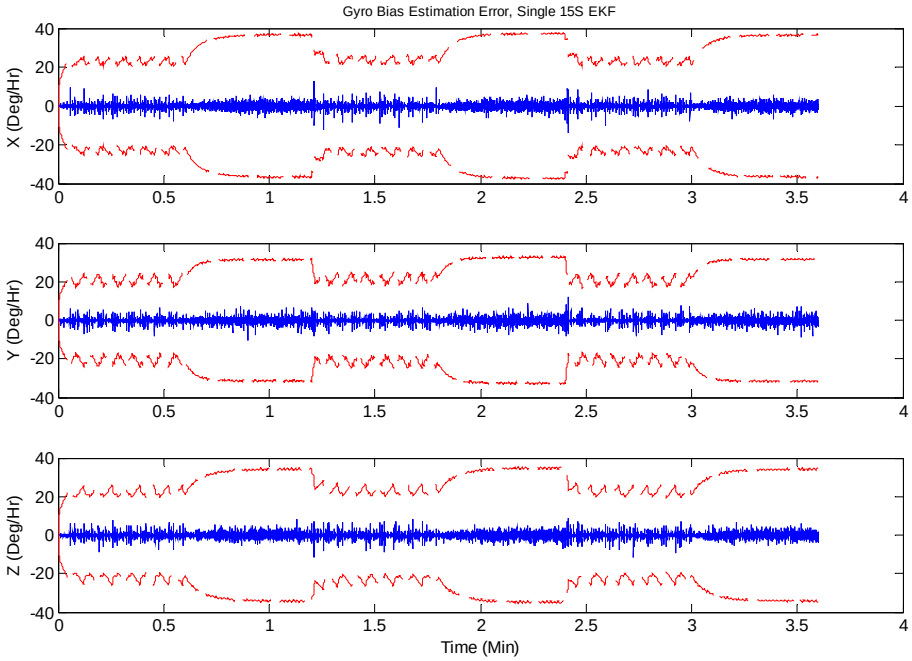

Figure 3. Gyro Bias Estimation Performance of a 15 State EKF

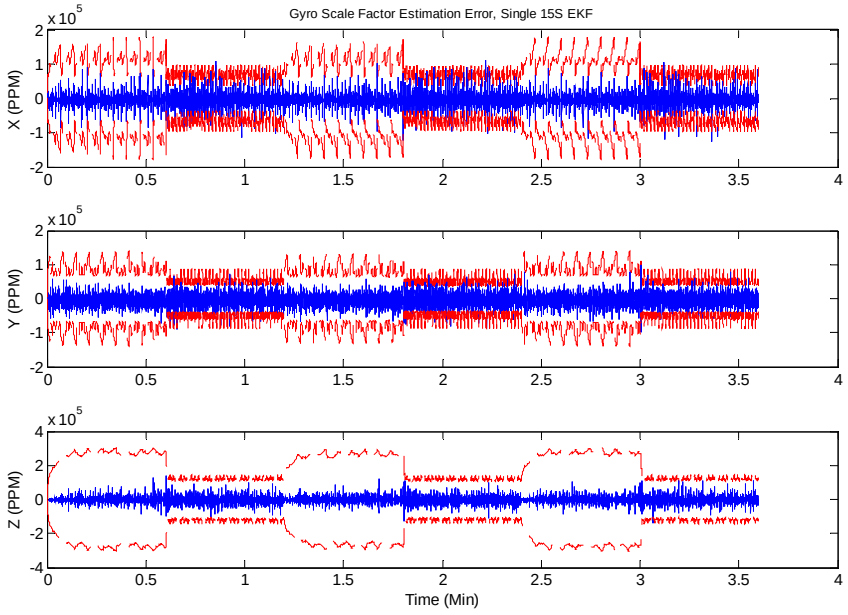

Figure 4. Scale Factor Estimation Performance of a 15 State EKF

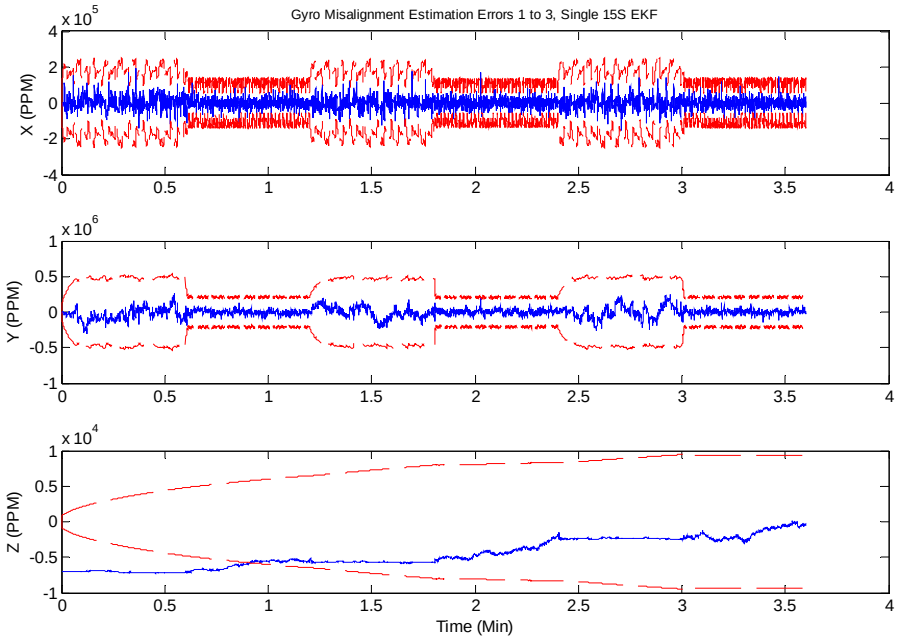

Figure 5. Upper Misalignment (MA) Error Estimation of a 15 State EKF (poor performance in estimating the 3rd upper misalignment error for the first two minutes)

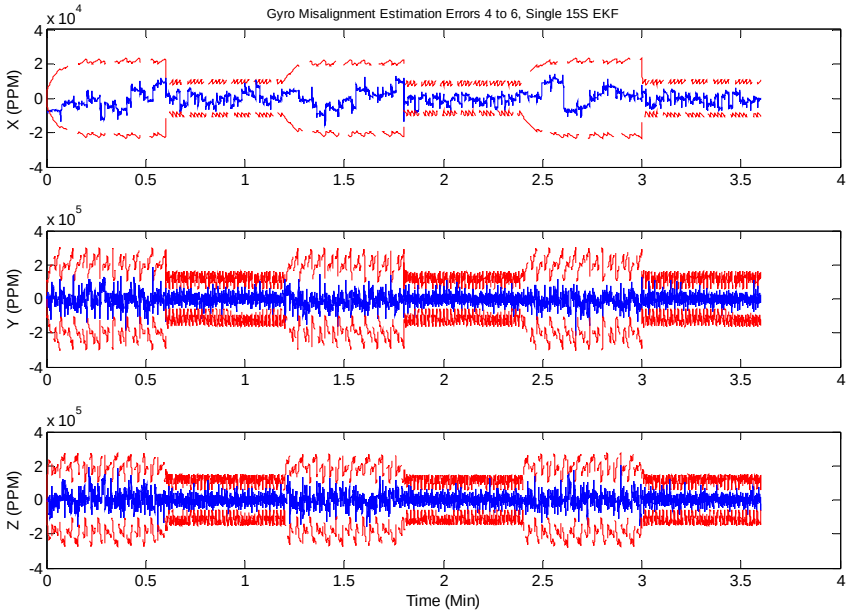

Figure 6. Lower MA Error Estimation of a 15 State EKF

5.2 Performance of Three EKFs MMAE Mixing Scheme (6 State, 9 State, and 15 State EKF Models)

Figures 7 to 12 present the performance of a three EKFs solution. The estimation of all gyro errors has been improved via the15 state EKF add-on (by quickly comparing the attitude estimation error responses presented in Figure 3 versus Figure 7). For the remainder of the gyro errors estimation, SF and MA error estimation accuracy is also relatively improved (i.e., Figures 9 to 11).

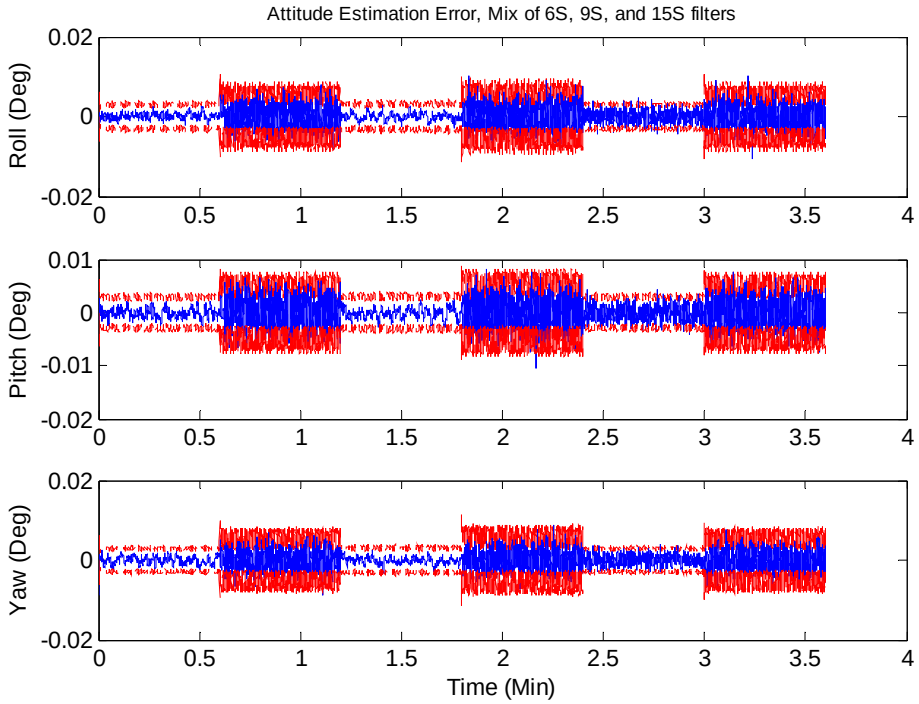

Figure 7. Attitude Estimation Via MMAE Mixing of Three EKFs (1 sigma error:[5.7247 5.5211 5.3248] arcsecs)

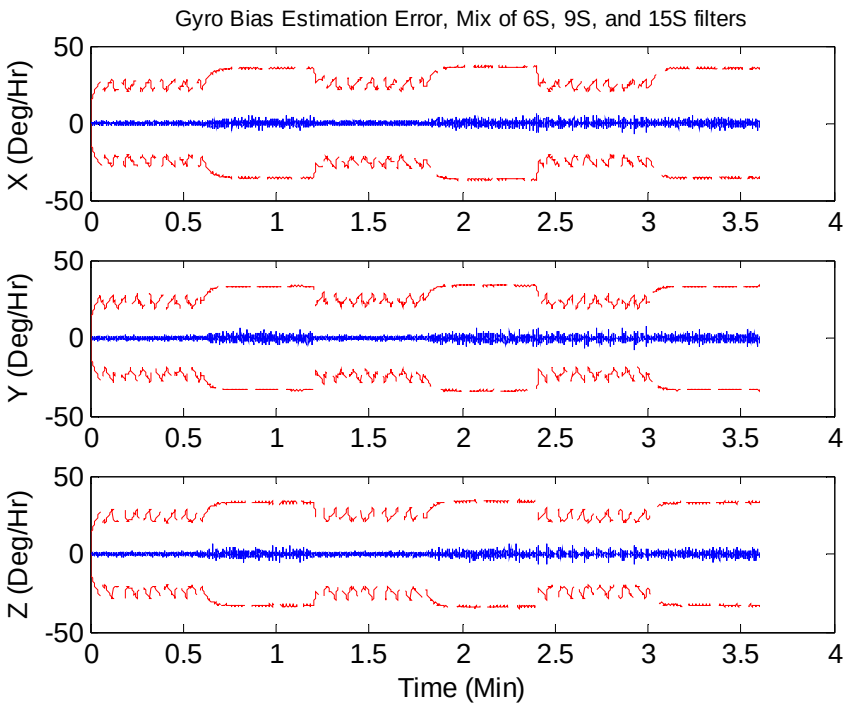

Figure 8. Gyro Bias Estimation via MMAE Mixing of Three EKFs

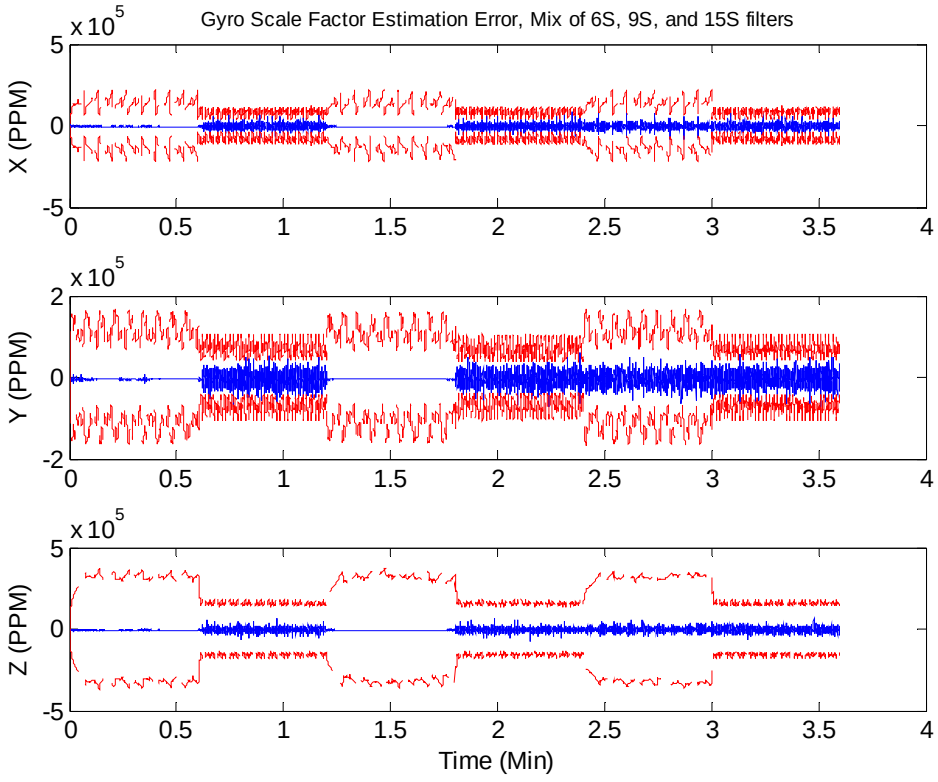

Figure 9: Gyro SF Error Estimation via MMAE Mixing of Three EKFs

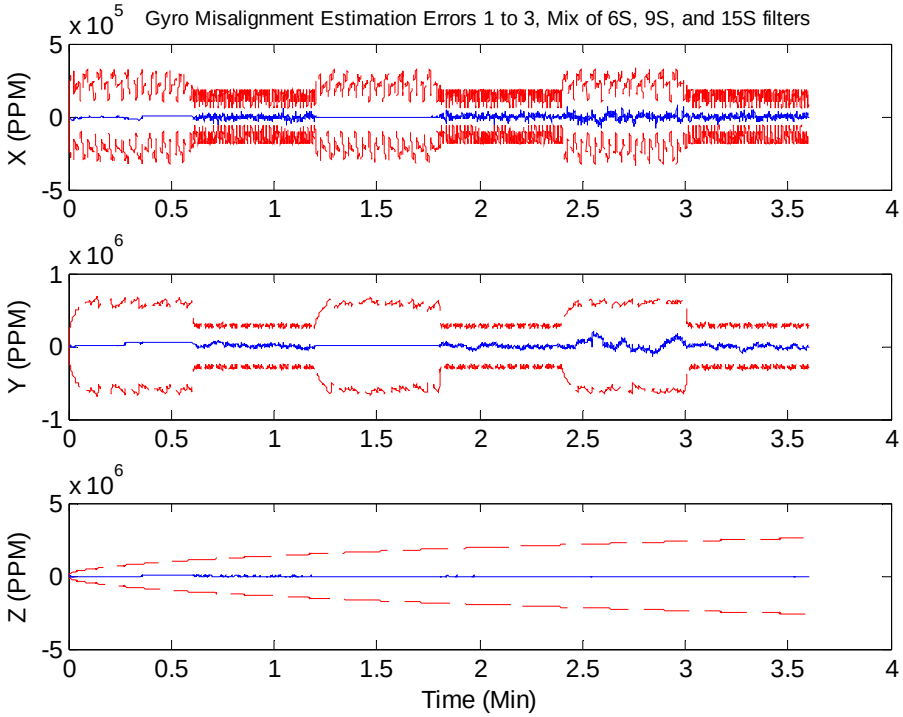

Figure 10. Gyro MA Error Estimation via MMAE Mixing of Three EKFs

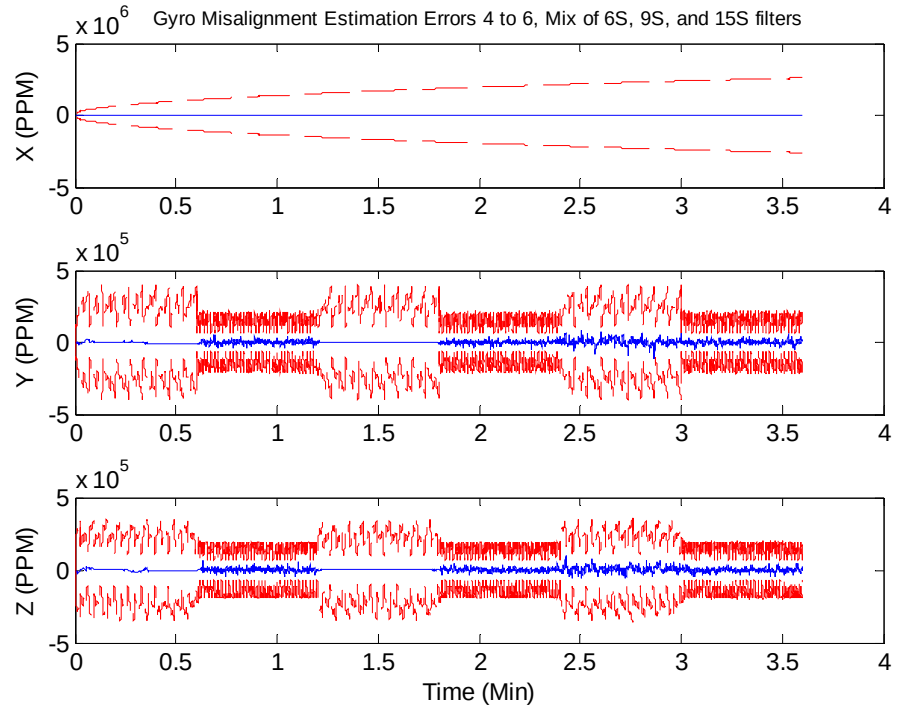

Figure 11. Gyro SF Error Estimation via MMAE Mixing of Three EKFs

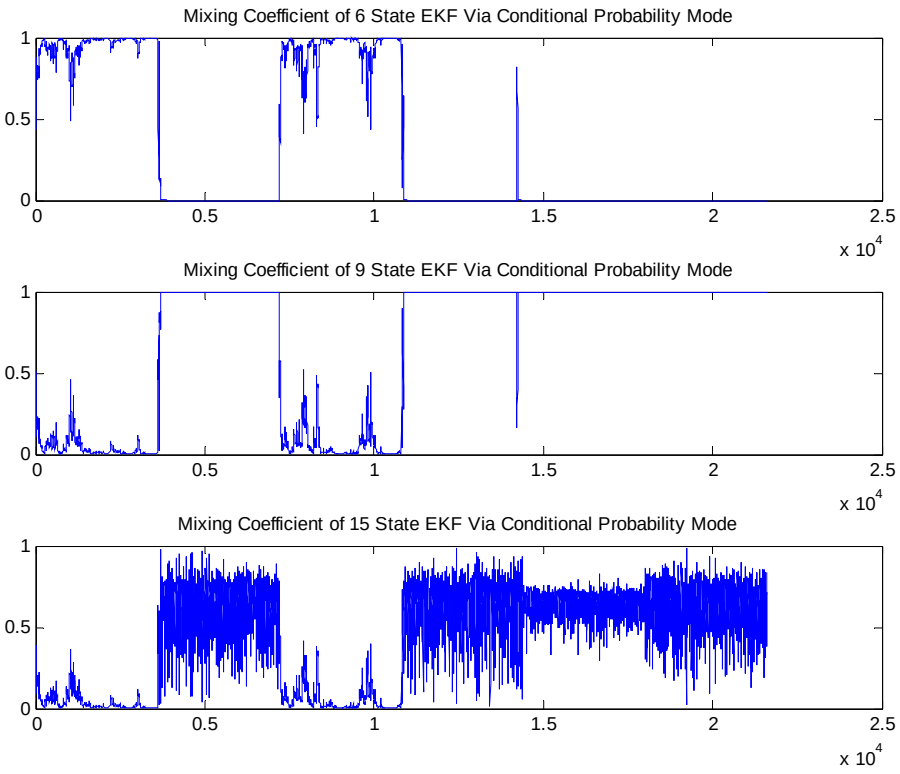

Figure 12. MMAE Mixing Coefficients of Three EKFs

5.3 Performance of Three EKFs MMAE with IMM Mixing Scheme (6 State, 9 State, and 15 State EKF Models)

The MMAE Mixing coefficients shown in Figure 12 are now replaced with the IMM mixing update scheme (via equation 32) to compute the new real-time mixing coefficients (see Figure 13) among three EKFs. Attitude estimation accuracy among three axes has been dramatically improved (see Figure 14) using the mixing coefficients computed by the IMM scheme. The performance of the IMM scheme shows that even with scale factor and misalignments, the best choice for the filter design is a combination of all three filters, i.e. using the 15 state filter only does not necessarily produce the best results. This is most likely due to the observability of the system. For example, at times of low observability estimation of misalignments is difficult, but the gyro biases may still be estimated well. The coupling of the gyro biases with the misalignments in the 15 state filter may produce worse results for gyro bias estimation that using only a 6 state filter. The IMM scheme provides a mechanism that yields the best possible performance.

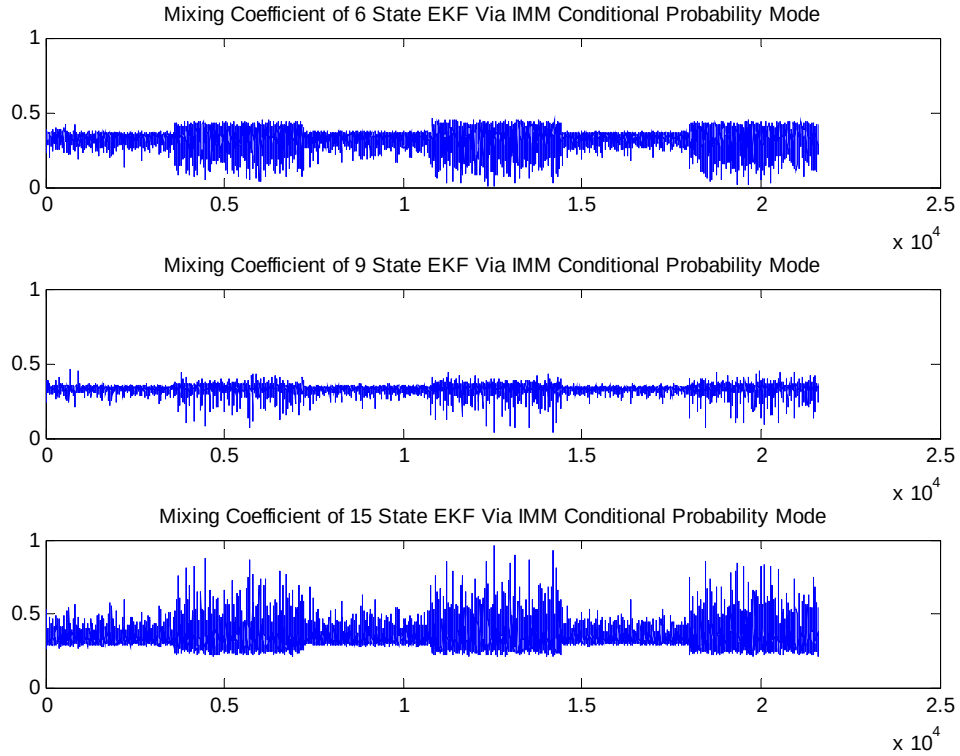

Figure 13. IMM Mixing Coefficients

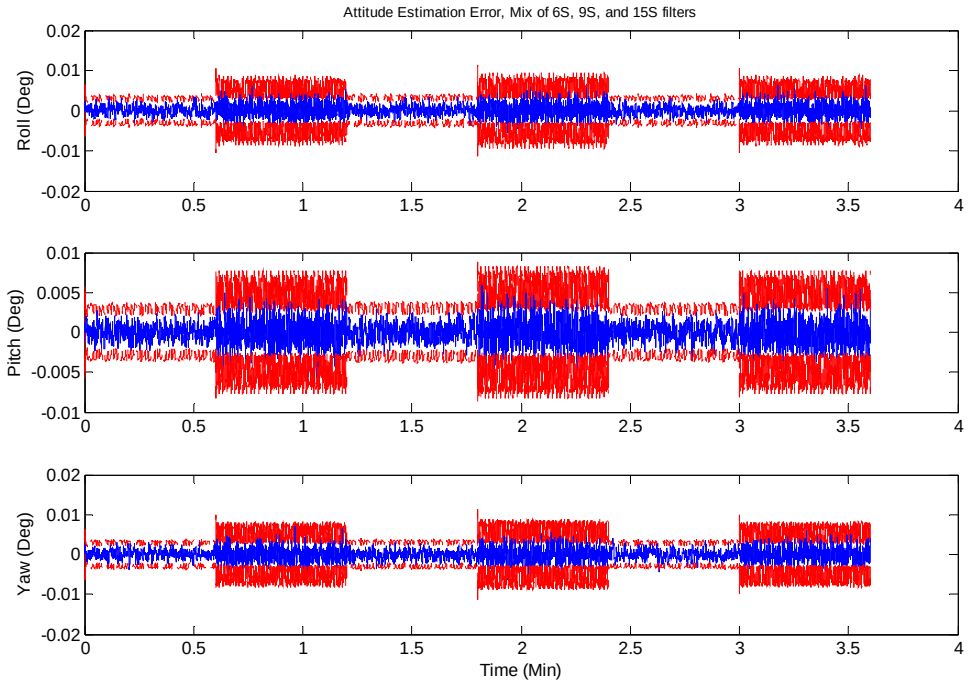

Figure 14. Improved Attitude Estimation Accuracy via IMM Mixing Coefficients (1 sigma error: [4.5570 4.3385 4.6461] arcsecs & its well behaved error response versus the attitude error response of a single 15 state EKF presented in Figure 2)

5.4 Performance Enhancement of MMAE/IMM Architecture with Inner Loop Gyro Noise Identification

The attractive baseline MMAE/IMM mixing architecture presented early on is then further enhanced with an "inner loop" subsystem implemented with pure MMAE algorithm (i.e., equations 18 to 28) to perform gyro noise identification. This adaptive dual-compensation MMAE estimation scheme is presented in Figure 15. They are clearly useful for MEMS IMU or IRU utilization in general for the low-cost high performance navigation subsystem design of future space vehicles.

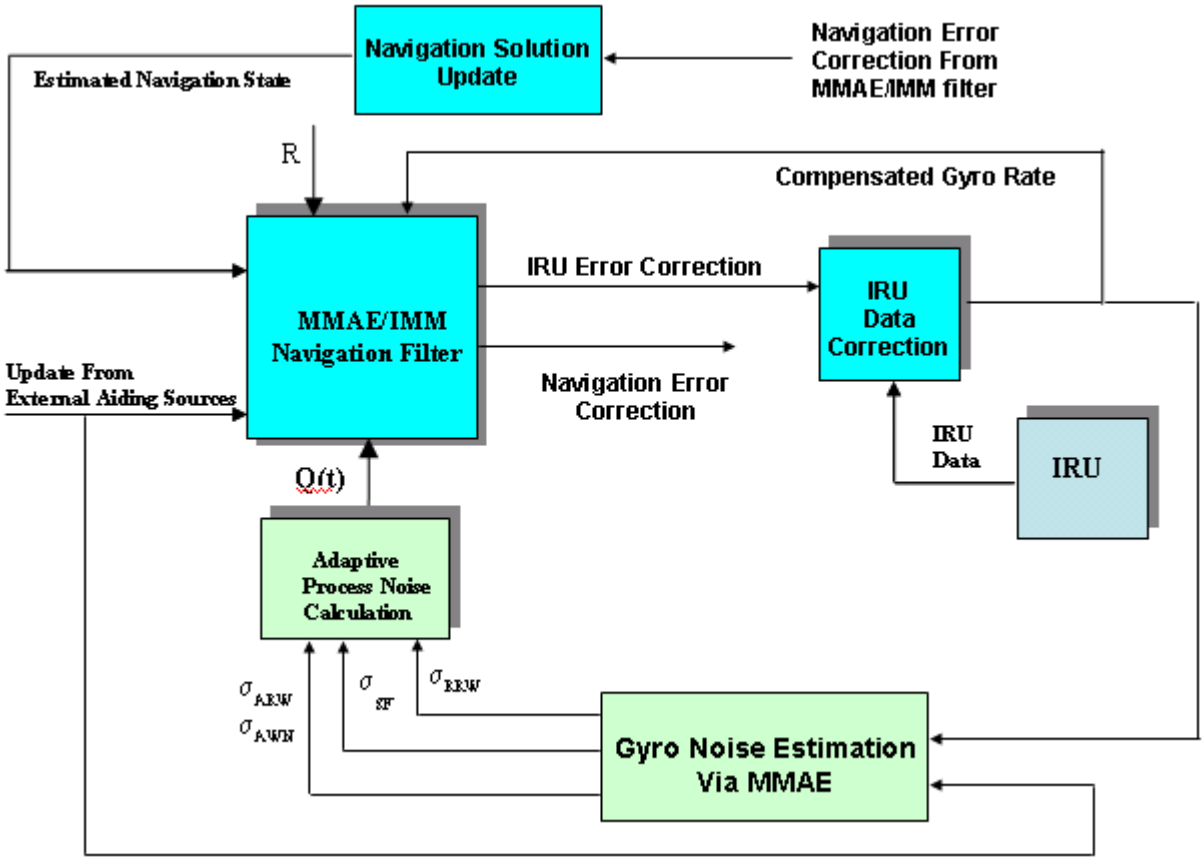

Figure 15. Dual-Compensation Architecture Supporting MEMS IRU Utilization

Figures 16 and 17 present the excellent gyro noise identification of the MMAE scheme implemented as a separate subsystem to estimate the IRU noise. Only rate random walk (RRW), angular random walk (ARW), and SF noises are estimated in this study. The one sigma values of RRW, ARW, and SF noises estimated online, will feed the adaptive process noise block to compute the right signature for the MMAE/IMM filter to effectively maintain the accuracy of the navigation solution in the presence of IRU performance degradation (due to aging or in-orbit drift variation).

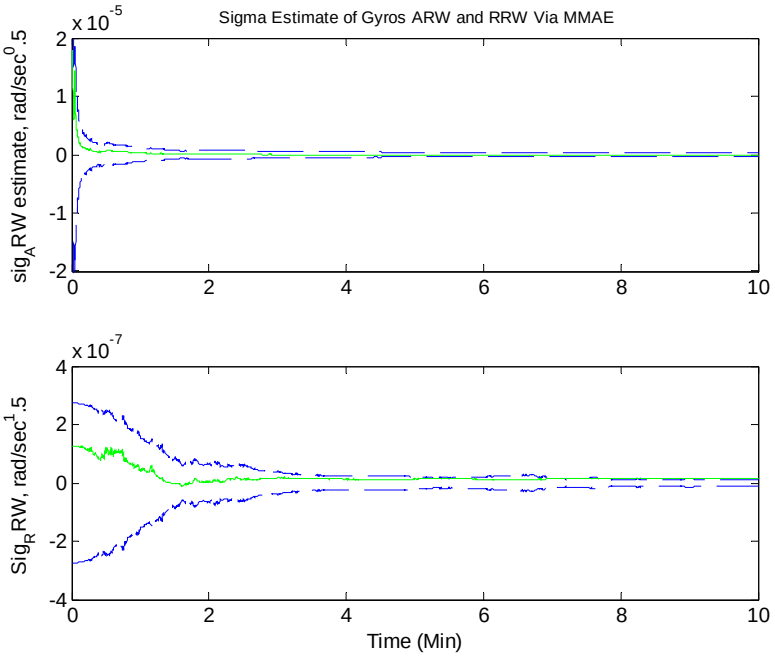

Figure 16. RRW and ARW Noise Estimation

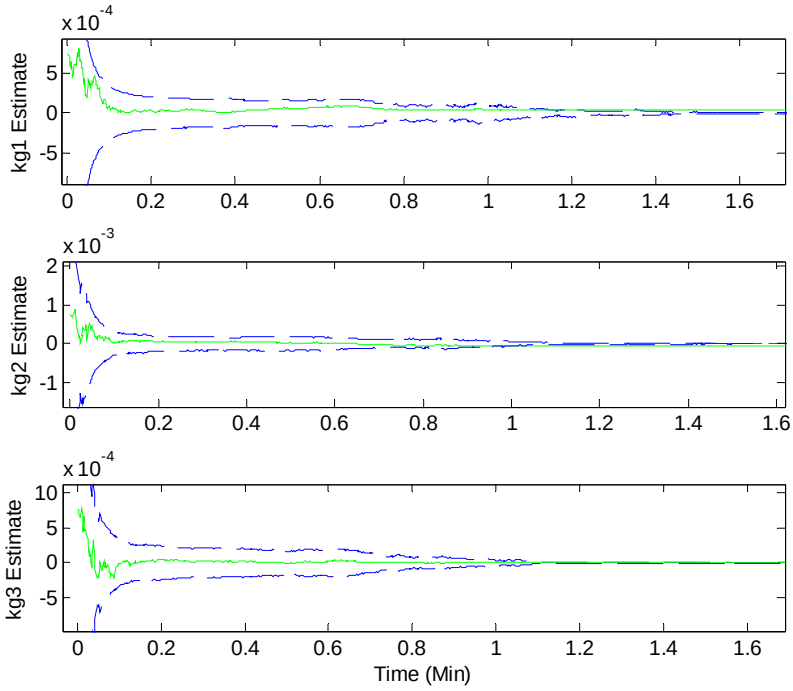

Figure 17. SF Noise Estimation

6.0 Conclusion

An adaptive filtering architecture via MMAE scheme is proposed to ameliorate the effect of gyro SF and MA errors at high rate operating condition and effectively maintain an accurate attitude estimation performance while a traditional EKF scheme suffers for a same operating condition. The MMAE scheme is exploited to offer two primary design features: (1) multiple EKF models mixing to provide the right fusion combination between various filter models' state vectors for a consistent navigation solution update at various rate magnitudes and (2) the ability to mix multiple external sensor data update in a simultaneous fashion via MMAE framework regardless their disparate update rate. In other words, external data available out of each sensor provided at different output rate can be systematically combined via the MMAE/IMM mixing scheme (e.g., ST/IRU data at 100Hz, radar altimeter data at 20Hz, and image based sensor data at 10Hz). Simulation performance results indicate that the MMAE/IMM provides better estimates compared to using each filter alone. Also, the MMAE approach is an effective scheme to estimate gyro noise parameters.

References

1. Lefferts, E. J., Markley, F. L., and Shuster, M. D., "Kalman Filtering for Spacecraft Attitude Estimation," *Journal of Guidance, Control, and Dynamics*, Vol. 5, No. 5, 1982, pp. 417–429.
2. Lam, Q. M. and Crassidis, J. L., "Precision Attitude Determination Using A Multiple Model Adaptive Estimation Scheme," *Proceedings of the IEEE Aerospace Conference*, Big Sky, Montana, March 2007.
3. Markley, F.L., Cheng, Y., Crassidis, J.L., and Oshman, Y., "Averaging Quaternions," *Journal of Guidance, Control, and Dynamics*, Vol. 30, No. 4, 2007, pp. 1193-1197.
4. Bar-Shalom, Y. and Li, R., *Estimation and Tracking: Principles, Techniques, and Softwares*, Artech House, 1993.
5. Lam, Q. M., Li, X. R., and Fujikawa, S.J., "Future Trends to Enhance the Robustness of a Target Tracker," *Proceedings of the AIAA GN&C Conference*, San Diego, CA July 1996.
6. Shuster, M. D., "A Survey of Attitude Representations," *Journal of the Astronautical Sciences*, Vol. 41, No. 4, 1993, pp. 439-517.